Conserved NPPB+ Border Zone Switches From MEF2- to AP-1-Driven Gene Program

van Duijvenboden, Karel; de Bakker, Dennis E. M.; Man, Joyce C. K.; Janssen, Rob; Günthel, Marie; Hill, Matthew C.; Hooijkaas, Ingeborg B.; van der Made, Ingeborg; van der Kraak, Petra H.; Vink, Aryan; Creemers, Esther E.; Martin, James F.; Barnett, Phil; Bakkers, Jeroen; Christoffels, Vincent M.

Published in:
Circulation

DOI:
10.1161/CIRCULATIONAHA.118.038944

Published: 01/01/2019

Citation for pulished version (APA):
van Duijvenboden, K., de Bakker, D. E. M., Man, J. C. K., Janssen, R., Günthel, M., Hill, M. C., Hooijkaas, I. B., van der Made, I., van der Kraak, P. H., Vink, A., Creemers, E. E., Martin, J. F., Barnett, P., Bakkers, J., & Christoffels, V. M. (2019). Conserved NPPB+ Border Zone Switches From MEF2- to AP-1-Driven Gene Program. *Circulation*, *140*(10), 864-879. https://doi.org/10.1161/CIRCULATIONAHA.118.038944

Circulation

ORIGINAL RESEARCH ARTICLE

Conserved *NPPB*+ Border Zone Switches From MEF2- to AP-1–Driven Gene Program

Karel van Duijvenboden, PhD*
Dennis E.M. de Bakker, MSc*
Joyce C.K. Man, MSc*
Rob Janssen, PhD*
Marie Günthel, Dipl-Ing*
Matthew C. Hill, PhD
Ingeborg B. Hooijkaas, MSc
Ingeborg van der Made, MSc
Petra H. van der Kraak, BS
Aryan Vink, PhD
Esther E. Creemers, PhD
James F. Martin, PhD
Phil Barnett, PhD
Jeroen Bakkers, PhD
Vincent M. Christoffels, PhD

BACKGROUND: Surviving cells in the postinfarction border zone are subjected to intense fluctuations of their microenvironment. Recently, border zone cardiomyocytes have been specifically implicated in cardiac regeneration. Here, we defined their unique transcriptional and regulatory properties, and comprehensively validated new molecular markers, including *Nppb*, encoding B-type natriuretic peptide, after infarction.

METHODS: Transgenic reporter mice were used to identify the *Nppb*-positive border zone after myocardial infarction. Transcriptome analysis of remote, border, and infarct zones and of purified cardiomyocyte nuclei was performed using RNA-sequencing. Top candidate genes displaying border zone spatial specificity were histologically validated in ischemic human hearts. Mice in which *Nppb* was deleted by genome editing were subjected to myocardial infarction. Chromatin accessibility landscapes of border zone and control cardiomyocyte nuclei were assessed by using assay for transposase-accessible chromatin using sequencing.

RESULTS: We identified the border zone as a spatially confined region transcriptionally distinct from the remote myocardium. The transcriptional response of the border zone was much stronger than that of the remote ventricular wall, involving acute downregulation of mitochondrial oxidative phosphorylation, fatty acid metabolism, calcium handling, and sarcomere function, and the activation of a stress-response program. Analysis of infarcted human hearts revealed that the transcriptionally discrete border zone is conserved in humans, and led to the identification of novel conserved border zone markers including *NPPB*, *ANKRD1*, *DES*, *UCHL1*, *JUN*, and *FOXP1*. Homozygous *Nppb* mutant mice developed acute and lethal heart failure after myocardial infarction, indicating that B-type natriuretic peptide is required to preserve postinfarct heart function. Assay for transposase-accessible chromatin using sequencing revealed thousands of cardiomyocyte lineage-specific MEF2-occupied regulatory elements that lost accessibility in the border zone. Putative injury-responsive enhancers that gained accessibility were highly associated with AP-1 (activator protein 1) binding sites. Nuclear c-Jun, a component of AP-1, was observed specifically in border zone cardiomyocytes.

CONCLUSIONS: Cardiomyocytes in a discrete zone bordering the infarct switch from a MEF2-driven homeostatic lineage-specific to an AP-1–driven injury-induced gene expression program. This program is conserved between mouse and human, and includes *Nppb* expression, which is required to prevent acute heart failure after infarction.

*Dr van Duijvenboden, D. de Bakker, J. Man, Dr Janssen, and M. Gunthel contributed equally.

Key Words: border zone ■ epigenomics ■ myocardial infarction ■ myocardium ■ sequence analysis, RNA ■ transcription

Sources of Funding, see page 878

https://www.ahajournals.org/journal/circ

Clinical Perspective

What Is New?

- Mouse myocardial infarctions are surrounded by an *Nppb*-positive border zone, which contains cardiomyocytes that are transcriptionally and epigenetically distinct from remote myocardium.
- Infarcted human hearts contain similar border zone cardiomyocytes that share expression of novel border zone markers including *NPPB*, *JUN*, *DES*, and *ANKRD1*, and are mainly located at the subendocardium adjacent to the infarction.
- *Nppb* knockout mice are unable to recover from an ischemic injury, illustrating the importance of processes that occur in the border zone.
- *Nppb*-positive border zone cardiomyocytes undergo a profound transcriptional and epigenetic reprogramming, switching from a MEF2 to an AP-1 (activator protein 1)–responsive gene program.

What Are the Clinical Implications?

- Using *Nppb* knockout mouse, we illustrate that processes activated in the border zone are required for recovery after myocardial infarction, which may be applicable to patients that had an ischemic injury.
- Here, we present novel border zone markers that can be used in clinical research and are candidate biomarkers for assessing infarction severity and state.
- Because border zone cardiomyocytes have recently been implicated as a source for cardiomyocyte regeneration, the identification of the human subendocardial border zone might lead to novel strategies focusing on stimulating these cardiomyocytes to regenerate the injured heart.

After acute myocardial infarction (MI), the compromised ischemic muscle is lost and replaced by scar tissue, impairing heart function. The mammalian heart is considered to be an essentially postmitotic organ with negligible regenerative capacity,[1] with cardiomyocyte (CM) hypertrophy serving as the principle adaptive response to injury. The infarct zone is usually highly irregular in shape, infiltrating the adjacent spared myocardium,[2] which comprises a mixture of viable, although severely affected CMs.[3] The increase in CM cell size and reduction in capillary density is greater in the region bordering the infarct zone than in the remote area. CMs closer to the injury show hallmarks of dedifferentiation, sarcomere depletion, and decrease in mitochondrial volume in comparison with remote CMs.[4,5] Molecular analyses of samples taken from different locations of the infarcted wall have consistently shown the existence of transcriptional differences between myocardium proximal and distal to the infarct.[6–9]

Pragmatically, the proximal-distal axis of the infarcted ventricular wall has been divided in an infarct zone (IZ), an infarct boundary zone or border zone (BZ; perfused but hypocontractile), and a remote zone (RM; perfused).[10] The BZ remodels electrophysiologically and can be the origin of ventricular tachycardia, which is a common cause of sudden cardiac arrest in patients after MI, which originates from the BZ.[11–13] Furthermore, the BZ may be more susceptible to additional ischemic episodes, and its hypocontractile property seemingly expands after MI to involve contiguous myocardium that progressively loses contractile function as the heart remodels.[10] Recently, the BZ myocardium received renewed attention with respect to its potential role in postinjury cardiac regeneration. Zebrafish efficiently regenerate the heart after injury, replacing the infarcted tissue by proliferating CMs, which are mainly located in the zone bordering the injury.[14] Furthermore, in transgenic mouse models of enhanced regeneration, CM proliferation is primarily seen in the region proximal to the infarct, ie, the putative BZ.[15–18] Here, we identified and characterized a transcriptionally distinctive *NPPB*-expressing BZ conserved in mouse and human, and observed a role for *Nppb* in the survival after MI. Our findings indicate that a CM lineage-specific MEF2-driven regulatory program is replaced by an AP-1 (activator protein 1)–driven stress-responsive program in BZ CMs.

METHODS

An expanded methods section is available in the online-only Data Supplement. The data, analytic methods, and study materials will be made available by the authors to other researchers for purposes of reproducing the results or replicating the procedure.

Mice

Animal care and experiments conform to the Directive 2010/63/EU of the European Parliament. All animal work was approved by the Animal Experimental Committee of the Academic Medical Center, Amsterdam, and was performed in compliance with the Dutch government guidelines.

BAC-Nppb-Katushka,[19] *Myh6-MerCreMer*,[20] and *nTnG* (JAX stock #023035) mice were bred on the FVB/N background. Tamoxifen (20 mg/kg) was administrated intraperitoneally 1 week before *t*=0 and repeated the 2 following days. Myocardial infarction was performed. Two independent *Nppb*-deficient mouse lines were generated by CRISPR/Cas9-mediated genome editing in FVB oocytes.

Human Material

Paraffin-embedded infarcted human heart tissue from 3 individuals who had died of MI were retrieved from the pathology archive of the University Medical Center Utrecht. Material was handled in a coded manner that met the criteria of the Code of Conduct used in the Netherlands for the responsible use of human tissue in medical research (www.federa.org/

codes-conduct). Collection of the archive material was approved by the local biobank review committee (protocol 15–252).

Statistical Analysis

Differential expression analysis was performed using the DESeq2 package.[21] *P* values were corrected for multiple testing using the false discovery rate method of Benjamini-Hochberg ($P<0.05$).

To compare the survival distributions between *Nppb*$^{-/-}$ mice and wild-type littermates after MI we used a log-rank test ($P<0.05$).

Motifs detected with HOMER were considered enriched when $P<1^{-10}$ was reached, as recommended by the authors (http://homer.ucsd.edu/homer/).[22]

To determine whether assay for transposase-accessible chromatin using sequencing (ATAC-seq) peak categories were differentially bound by transcription factors (TFs), we counted the number of chromatin immunoprecipitation sequencing (ChIP-seq) tags present per peak. To test for differences between groups a one-way ANOVA was performed by using a multicomparison procedure post hoc Games-Howell test ($P<0.05$). We performed a log-transformation on the ChIP-seq count data when the counts were not normally distributed.

Data Availability

All RNA-sequencing (RNA-seq) and ATAC-seq data have been deposited at the Gene Expression Omnibus under the accession number (GSE110209); and PCM-1 (pericentriolar material 1; GSE128034) and *Nppb*$^{-/-}$ (GSE128196) RNA-seq data. An Excel file has been made available in the online-only Data Supplement that contains tables with candidate BZ genes with the use of various criteria.

RESULTS

Identification of 3 Transcriptionally Distinct Zones in the Injured Ventricular Wall

To assess the spatial distribution of the transcriptome in the injured heart, we permanently ligated the left anterior descending coronary artery in 10- to 12-week old mice. *Col1a1* and *Tnni3* expression patterns typically marked the IZ and myocardium, respectively. *Nppa* expression, marking a BZ region,[19] was evident in the area adjacent the infarcted area and overlapping the spared myocardium (Figure 1A and 1B). The *Nppa*-negative myocardium was considered to be the RM. The spatial analysis of the *Katushka* and *Nppa*/*Nppb* patterns in *BAC-Nppb-Katushka* mice 7 days postinfarction (dpi) revealed that the transition of expression between the BZ and RM was relatively sharp rather than gradual, indicating that the BZ is a discrete region adjacent to the infarct. Moreover, the size of the BZ was relatively constant across varying infarct sizes (Figure 1C). The thickness (from IZ to RM) of the *Nppa*/*Nppb*-positive zone was between 0.2 and 0.7 mm (Figure 1B and 1C and data not shown). The discreteness and sizes of the zones made it possible to isolate each zone by microdissection for characterization by RNA-seq analysis. Three independent samples of RM, BZ, and IZ of 3, 7, and 14 dpi hearts were microdissected, and the *Nppa* expression level in the microdissected tissues was compared with sham-operated left ventricular tissue to confirm correct dissection and isolation of the respective zones (Figure 1D). With the use of unsupervised principal component analysis, segregation between samples by time points and zones was observed. Based on overall expression patterns, all sham samples clustered together, followed by RM, BZ, and IZ. It is interesting to note that the samples harvested 3 days after left anterior descending coronary arteries were separated from both other time points, which were more similar to each other (Figure 1E).

Characterization of the Transcriptional Response of the BZ

Comparison of the transcriptomes of the BZ and RM at different time points than those of sham tissue showed that the majority of differentially expressed genes (3563) originated from the BZ (2983 genes), whereas the contribution of differentially expressed genes solely in the remote ventricular wall was minor (Figure 1F and Figure I in the online-only Data Supplement). The direction of change of differentially expressed genes in RM and BZ was the same, ie, either up in both zones or down in both zones, indicating that the injury responses of the BZ and RM are comparable, but much more extensive in the BZ (Figure I in the online-only Data Supplement). The early response involved the highest number of genes and stabilized thereafter as shown by increased gene overlap (Figure 1G). Analysis of changes in Kegg pathways and GO terms between different time points and zones was concordant with the course of pathology (eg, at 3 days postinjury a dominant inflammatory response was noted; Figure 1H, clusters 3–5). In the BZ, downregulated genes were enriched for CM-specific genes (sarcomere, calcium handling), whereas upregulated genes were enriched for those known to be expressed in non-CMs, compatible with the invasion of immune cells and activation of fibroblasts after injury.[12,23,24] Moreover, a strong cell-cycle activation response, probably derived from activated fibroblasts and immune cells, was observed at 3 dpi (Figure 1H, cluster 5).

Cluster analysis revealed a set of 165 TF–encoding genes induced in the BZ (Figure II in the online-only Data Supplement and Table I in the online-only Data Supplement). These include *Jun* and *Fosl2*, encoding components of the AP-1 complex that regulates a wide range of cellular processes, including cell proliferation, death, survival, and differentiation.[25–27] Fur-

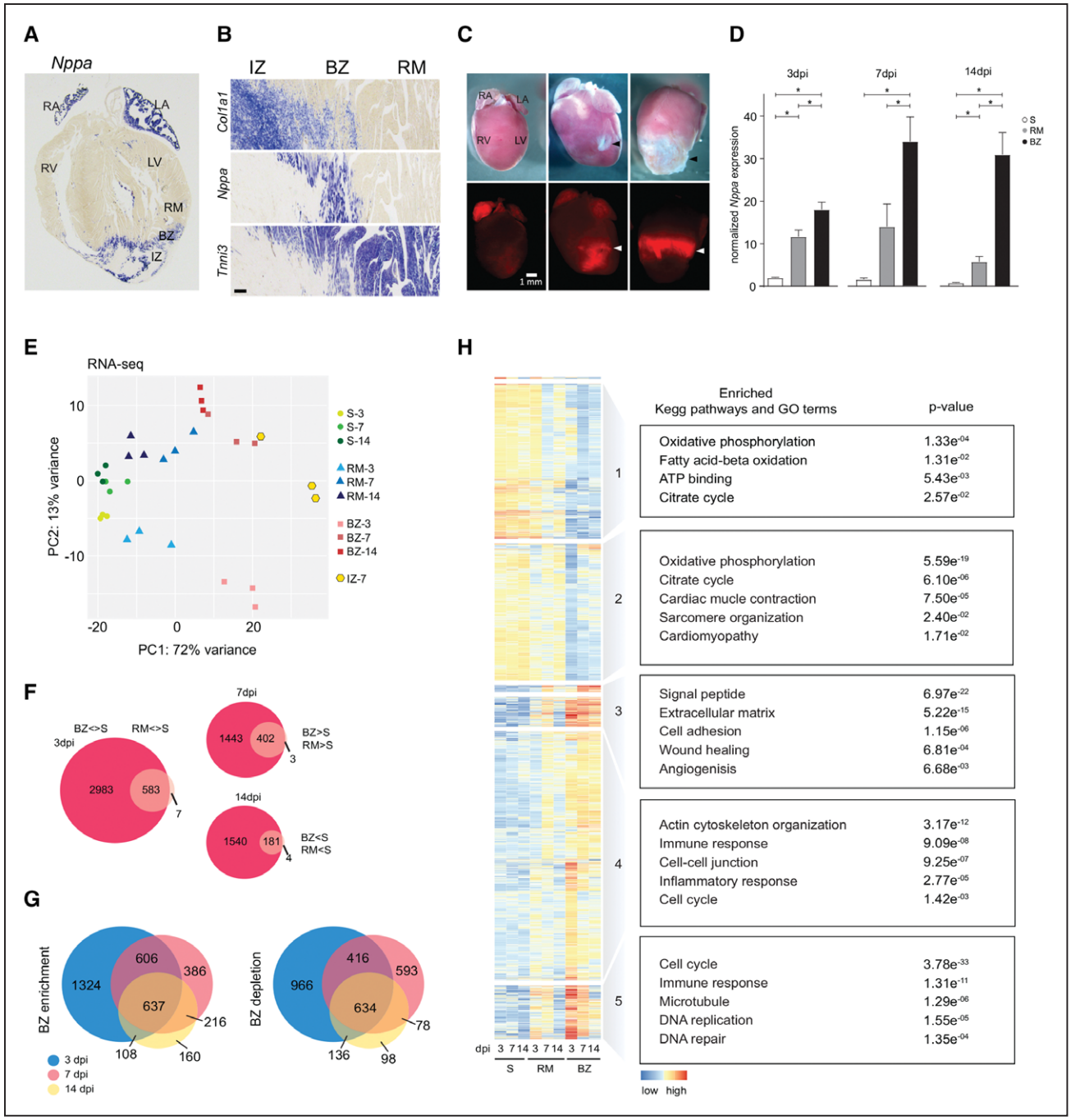

Figure 1. RNA-sequencing identifies the border zone based on a distinct expression profile on microdissected LV tissue.
A, In situ hybridization analysis showing the expression pattern of *Nppa* in the 7 dpi heart. **B**, Spatial expression patterns and corresponding in situ hybridization of 3 references genes *Col1a1*, *Nppa*, and *Tnni3* at 7 dpi. *Nppa* expression highlights the BZ. **C**, Light (**Upper**) and fluorescent microscopic pictures (**Lower**) of hearts of 7 dpi *BAC-Nppb::Katushka* mice, revealing the relatively sharply defined BZ (white arrowheads) around both a small and large infarct area (black arrowheads). **D**, After microdissection of the BZ and RM, *Nppa* expression was assessed by quantitative polymerase chain reaction and compared with control sham hearts. Values are means±SEM; **P*<0.05. **E**, Principal component analysis clustered the microdissected LV tissue by zone and time postinjury. Samples from different zones and time points are designated by colors. **F**, Comparison of differentially expressed genes of BZ (n=3) and RM (n=3) to sham (n=3) at 7 dpi showed that the majority of differentially expressed genes originate from the BZ. **G**, The set of differentially expressed genes of BZ tissue was cross-referenced with data obtained from infarcted LV tissue to highlight those differentially expressed genes that potentially play a part in the cardiomyocyte response to injury. **H**, Functional annotation heatmap of sham, RM, and BZ at different time points (n=3 per time point per tissue) based on differentially expressed genes sham versus BZ. BZ indicates border zone; dpi, days postinfarction; IZ, infarct zone; LA, left atrium; LV, left ventricle; RA, right atrium; RM, remote zone; and RV, right ventricle.

thermore, a number of genes (587) encoding excreted proteins were induced in the BZ that are candidate biomarkers (eg, *Clu*, *Gpx3*; Table II in the online-only Data Supplement).

The (post-MI) ventricular wall is composed of many different cell types.[9,12,23,24,28] To gain insight into the CM-specific response to injury, we purified CM nuclei from the BZ and RM by using PCM-1–mediated purification

(Figure 2 and Figure IIIA and IIIB in the online-only Data Supplement). In comparison with whole tissue samples, PCM-1–sorted samples were enriched for cardiac genes and showed a low expression of genes specifically expressed by fibroblasts, endothelial cells, and leukocytes (Figure IIIC in the online-only Data Supplement). As also seen for the RNA-seq of whole tissue, the majority of significantly differentially expressed genes originates from cells of the BZ (Figure 2A). Genes upregulated in BZ CMs include the known markers *Nppa* and *Nppb*.

We compared the BZ and RM PCM-1+ nuclear RNA-seq data with those obtained from adult CMs from uninjured hearts[29] by using unsupervised hierarchical clustering (Figure 2C). Samples from the RM clustered together with CMs from uninjured heart, whereas the BZ samples cluster alone. GO term analysis of each gene cluster revealed that CMs in the BZ downregulate genes involved in processes like oxidative phosphorylation, citrate cycle, and lipid metabolism, whereas they upregulate genes involved in regulating transcriptional regulation, cell-cell adherens junctions, and hypertrophy. Cross-analysis with dissected BZ and PCM-1–sorted BZ samples indicated that *Clu*, *Gpx3, Flnc, Des, Fhl1, Serpine1, Synpo2l*, and *Ankrd1* are bona fide BZ markers confirmed in both experiments (Figure 2B). With the use of in situ hybridization, the BZ CM-specific induction of several markers at 7 dpi was validated (Figure 2D). Information regarding their function is provided in the in the online-only Data Supplement. Taken together, we present a rich data set analysis that can be used as a starting point for future studies on BZ-restricted processes.

BZ CMs Partially Revert to a Neonatal CM State

To gain insight into the state of differentiation of the BZ and RM, we compared our tissue and PCM1+ CM RNA-seq data sets with those from isolated neonatal and adult CMs.[29] The BZ profiles clustered with those of neonatal CMs (Figure IVA in the online-only Data Supplement). The RM and sham profiles clustered with those of adult CMs, indicating that RM does not dedifferentiate significantly after injury, in keeping with previous observations.[30] Scatter plot and GO term analysis (Figure IVB in the online-only Data Supplement) revealed that genes expressed at lower levels in neonatal, and BZ CMs, as well, are involved in oxidation-reduction processes and lipid metabolism. Genes expressed at higher levels in neonatal CMs and BZ CMs control transcription and cell-cell adherent junctions. However, many genes expressed at higher levels in neonatal CMs were not upregulated in BZ CMs, including genes involved in cell cycle regulation. Taken together, BZ CMs partially revert to the immature state of neonatal CMs.

Identification of the BZ in Human Infarcted Hearts

Next, we addressed whether a conserved transcriptional BZ could be identified in the ischemic human heart. Histological analysis of human cardiac tissue samples from individuals that experienced an MI (n=3) identified areas of coagulation necrosis of CMs, compatible with MI of 1 to 3 days after coronary artery occlusion, and collagen-rich areas, compatible with MI scars of ≥2 months (Figure 3A). The infarcted areas of selected samples were located in the subendocardial region of the left ventricle or intraventricular septum. These locations were confirmed by immunostaining against C4d, an excreted complement factor that is specific to necrotic CMs[31] (Figure 3B). Most of the surviving myocardium was found in the compact myocardium, away from the infarcted area, or in oxygenated perivascular and subendocardial regions (Figure 3A, orange). Areas of surviving myocardium toward the epicardial layer were considered to be RM.

A number of genes with region-specific expression in the mouse heart were selected for spatial expression analysis. Most tested BZ-induced genes (eg, *NPPA*, *NPPB*, *ANKRD1*, *DES*, *UCHL1*, *JUN*, *MYH7*, and *FOXP1*) showed similar expression patterns in the infarcted human hearts, with consistent but low expression in-between the IZ and the RM (Figure 3C, arrows) and around blood vessels with presumed residual blood flow (Figure 3C, stars). It is interesting to note that the strongest expression of the examined genes was observed in the *NPPA*-positive BZ CMs located in-between the IZ and the endocardium (Figure 3C and 3D and Figure VA in the online-only Data Supplement). This strong subendocardial expression was observed in all 3 ischemic heart samples that were investigated (Figure VB through VD in the online-only Data Supplement). The size of the subendocardial BZ was consistently ≈0.4 mm, similar to the BZ size in mouse hearts. The RM-specific, sarcomeric genes *ECH1* and *TCAP* showed strong expression in the RM and weak expression in the *NPPA*-positive subendocardial BZ region (Figure 3D and Figure VA in the online-only Data Supplement).

The histological analysis identified regions that experienced a recent MI (1–3 days old, C4d- and fibrin-positive) and regions with older fibrotic scars (collagen-positive, C4d-negative). A consistently higher expression of BZ genes was observed in CMs in close proximity to recent infarcted areas (fibrin-positive) in comparison to their expression levels in CMs close to older collagen-rich scars within the same heart (Figure VI in the online-only Data Supplement), indicating that expression of BZ genes in human MI hearts is temporally regulated. We conclude that, in the ischemic injured human heart, a distinct BZ is formed that is most pronounced at the subendocardial location, comprising CMs with high

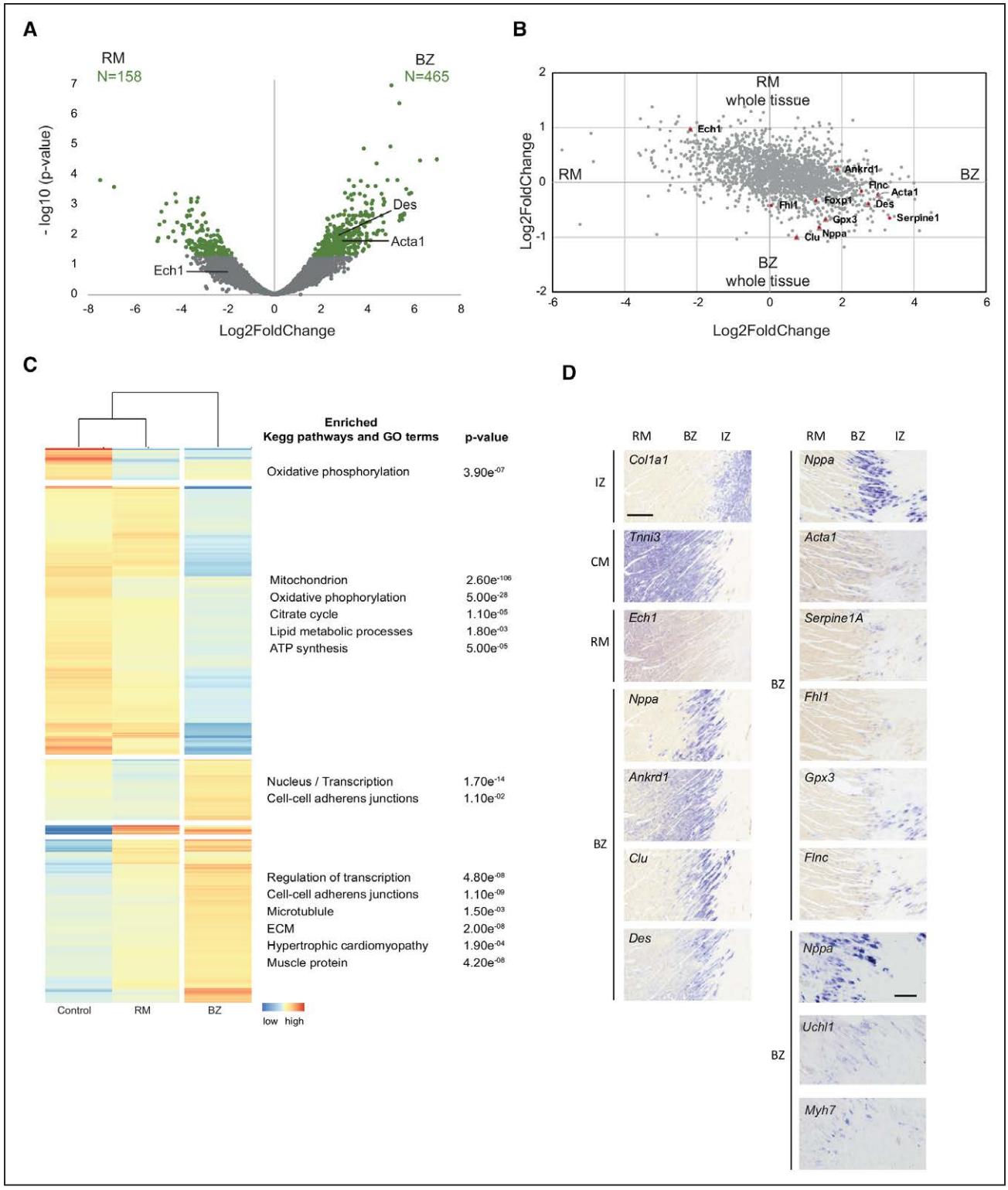

Figure 2. Gene expression in border zone cardiomyocytes.
A, Volcano plot showing cardiomyocyte nuclear transcripts differentially expressed between remote myocardium (RM; n=2) and border zone (BZ; n=3) tissues. Green dots indicate significantly differentially expressed genes (*P* adjusted for multiple testing: false discovery rate<0.05). **B**, Scatter plot of differentially expressed genes (Log2FoldChange) between the RM and BZ samples. **C**, Unsupervised functional annotation heatmap of control,[29] RM, and BZ samples. Gene ontology analysis was performed on each cluster. **D**, In situ hybridization shows the 3 reference genes: *Col1a1* for the infarct zone (IZ), *Tnni3* for cardiomyocytes, and *Ech1* for the RM. *Nppa* marks the BZ. New markers of the BZ resemble the expression pattern of *Nppa*. Scale bar, 0.5 mm and 0.1 mm (**right**, **lower panel**). CM indicates cardiomyocyte; and ECM, extracellular matrix.

expression of BZ markers involved in processes such as the stress response (*JUN*, *JUNB*, *ANKRD1*), development and proliferation (*NPPA*, *NPPB*, *FOXP1*) and muscle structure (*MYH7*, *DES*), and reduced expression of metabolic and sarcomeric genes (*ECH1*, *TCAP*). Based on the similar presence of these marker genes in the

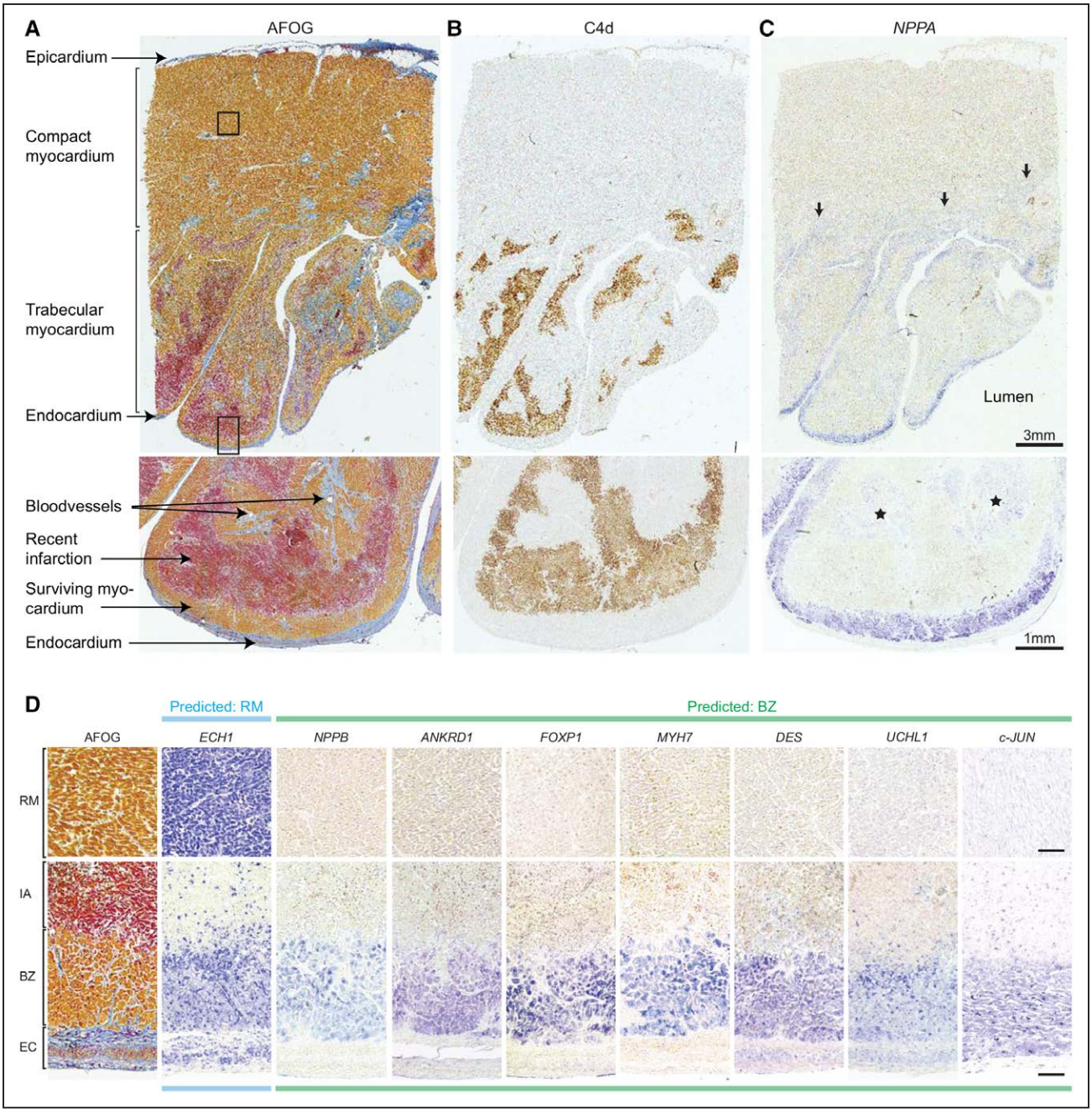

Figure 3. Human ischemic hearts show most pronounced expression of border zone markers in the subendocardium.
A, Acid fuchsin orange G (AFOG) staining on human heart tissue showing a large myocardial infarction. AFOG marks cytoplasm (orange), elastic fibrin (red), and collagen fibrils (blue). Elastic fibrin is indicative of coagulation necrosis, thus revealing a nontransmural recent infarction (red). In addition, collagen depositions suggest previous cardiac insults (blue). Black boxes indicate zoom locations for **D**. **B**, Anti-C4d antibody staining on a consecutive section marking necrotic cardiomyocytes overlying the fibrin-rich region. **C**, In situ hybridization against *NPPA* on a consecutive section. *NPPA* expression was observed in regions adjacent to the fibrin, including light staining in regions in the compact muscle layer (marked by arrows) and around blood vessels (marked by stars). Most pronounced staining is found at the surviving cells of the subendocardium. **D**, Zoom of the remote myocardium (RM) and the subendocardial region, including the injury area (IA), border zone (BZ), and endocardium (EC). In situ hybridization on consecutive sections confirmed expression of *ECH1* in RM. Predicted BZ genes showed specific expression in subendocardial myocardium. Scale bars, 100 µm.

injured mouse heart, we conclude that these injury-responsive processes are evolutionarily conserved.

Nppb Is Required During Recovery From MI

To gain insight into the role of the BZ-induced transcriptional program, we investigated the role of the conserved BZ gene *Nppb* after MI. We generated 2 independent *Nppb* knockout mouse lines by using CRISPR/Cas9 genome-editing technology (Figure 4A and Figure VII in the online-only Data Supplement). To assess to what extent our *Nppb* knockout model is affected, we performed RNA-sequencing of adult left ventricles of wild-type (n=4) and $Nppb^{-/-}$ mice (n=4).

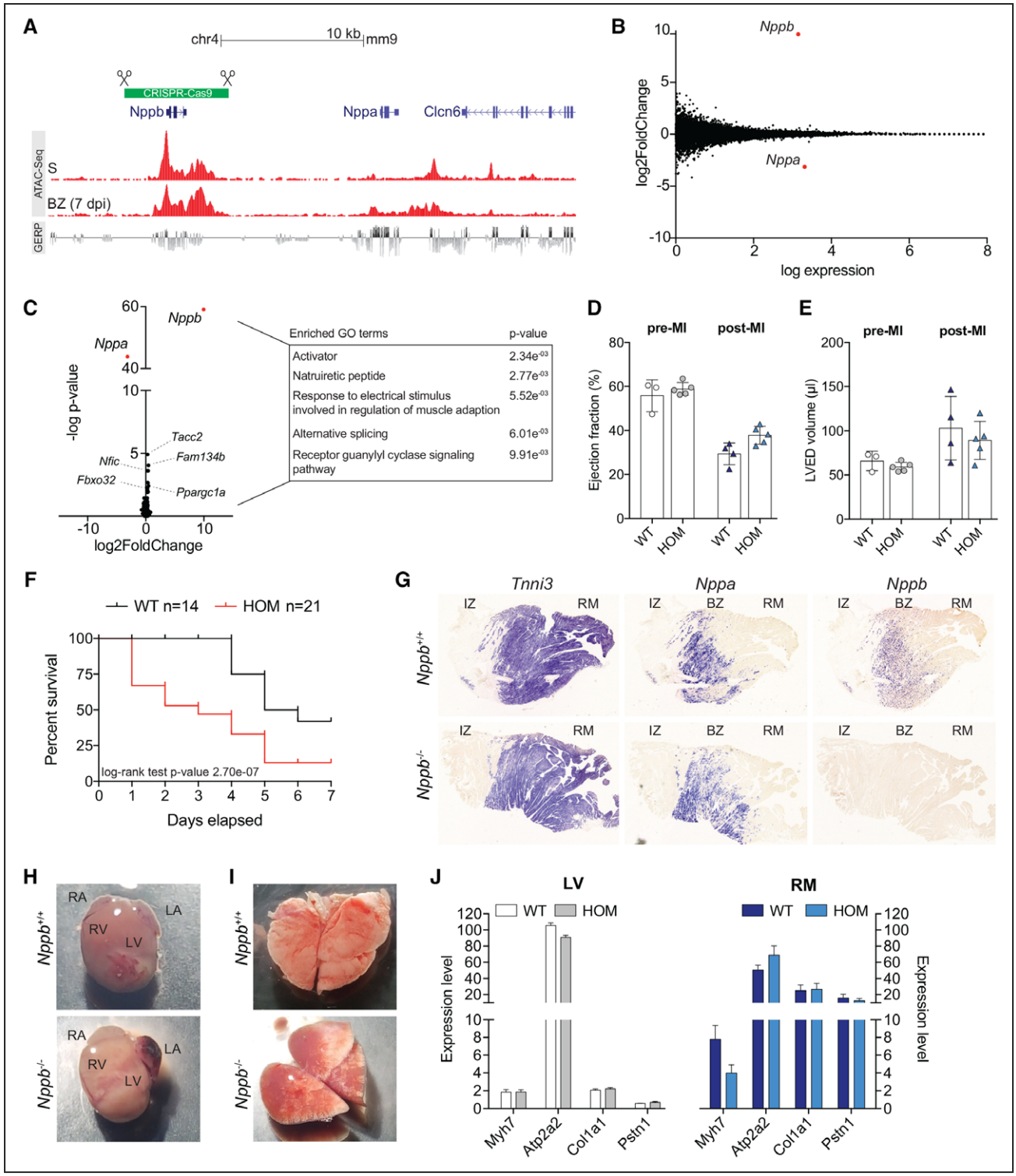

Figure 4. *Nppb* is required during recovery of myocardial infarction.

A, *Nppb* was targeted by using CRISPR/Cas9 genome-editing technology. **B**, MA plot showing ≈15 000 transcripts detected in wild-type (WT) LV (n=4) and *Nppb*$^{-/-}$ (HOM) LV (n=4). *Nppa* is significantly upregulated in HOM LV. **C**, Volcano plot showing significantly differentially expressed genes in HOM LV (*P* adjusted for multiple testing: false discovery rate <0.05). Included gene ontology analysis of several genes shown in the volcano plot. **D** and **E**, Echocardiographic parameters showing ventricular function: ejection fraction and left ventricular end-diastolic volume (LVED) pre-MI (WT n=3; HOM n=5) and post-MI (WT n=4; HOM n=5) at 7 dpi. **F**, Kaplan–Meier survival curve of HOM mice (n=21) and WT littermates (n=14) showed significant difference in survival (log-rank test *P*=2.70e–07). **G**, In situ hybridization analysis showing the expression pattern of *Tnni3*, *Nppa*, and *Nppb* in HOM mouse and WT at 7 dpi. **H** and **I**, Whole heart and lung of a HOM mouse presenting acute heart failure and a WT. **J**, After microdissection of RM (WT n=6; HOM n=6), expression of hypertrophy markers (*Myh7* and *Atp2a2* [SERCA2A]) and fibrosis markers (*Col1a1* and *Pstn*) were assessed by quantitative polymerase chain reaction and compared with left ventricular tissue (WT n=6; HOM n=6). Values are means±SEM. ATAC-seq indicates assay for transposase-accessible chromatin using sequencing; BZ, border zone; dpi, days postinfarction; GERP, Genomic Evolutionary Rate Profiling; IZ, infarct zone; LA, left atrium; LV, left ventricle; MA plot, Bland-Altman plot; MI, myocardial infarction; RA, right atrium; RM, remote zone; and RV, right ventricle.

Consistent with previous findings,[32] *Nppa* was significantly upregulated (Figure 4B). It is surprising that only 27 additional genes were mildly differentially expressed in *Nppb*$^{-/-}$ mice (Figure 4C). We could not identify any fibrosis markers among the differentially expressed genes in *Nppb*$^{-/-}$ mice, did not observe fibrotic lesions (Figure VIIIC and VIIID in the online-only Data Supplement), and did not observe differences in left ventricular systolic and diastolic function between genotypes (Figure 4D and 4E and Figure VIIIE through VIIIL in the online-only Data Supplement).

To assess the function of *Nppb* after injury, we subjected *Nppb*$^{-/-}$ mice and wild-type littermates to MI surgeries. *Nppb*$^{-/-}$ mice of both independent transgenic lines died more frequently shortly after MI because of acute heart failure (Figure 4F and Figure VIIA in the online-only Data Supplement). *Nppb*$^{-/-}$ mice that did not die of rupture presented shortness of breath, excess fluid in chest cavity and fluid leakage from the nose, blood coagulation in the left atrium (Figure 4H), and white spots that were found locally on the lungs (Figure 4I), in line with the occurrence of acute heart failure. These heart failure symptoms were not observed in wild-type mice after MI. No differences between genotypes were observed in relative heart weight, left ventricular function, or left atrial dimensions at 1 dpi between the 2 genotypes (Figure 4D and 4E and Figure VIIIB and VIIIE through VIIIJ in the online-only Data Supplement). Left ventricular diastolic parameters at 3 dpi showed a significant decrease in left ventricular internal diameter and left ventricular volume in *Nppb*$^{-/-}$ mice in diastole in comparison to wild type (Figure VIIIK and VIIIL in the online-only Data Supplement).

Both before and after MI, we did not find differences between genotypes in ventricular expression levels of myocardial hypertrophy markers (*Myh7* and *Atp2a2* [SERCA2A]) or fibrosis markers (*Col1a1* and *Pstn*; Figure 4J). A more detailed description of the data is provided in the in the online-only Data Supplement. Together, these findings suggest that *Nppb*$^{-/-}$ mice do not show a baseline phenotype but die 1 to 3 days after MI because of acute heart failure, indicating the requirement of induced *Nppb* expression to survive acute cardiac injury. This illustrates the importance of a BZ-induced gene program after MI.

Dynamic Epigenetic Landscape in the BZ CMs

Chromatin accessibility patterns reveal positions in the genome of actively engaged regulatory DNA elements, ie, promoters, enhancers, repressors, and insulators. We assessed how open chromatin states differ across homeostatic (sham) and 4, 7, and 14 dpi BZ CMs in vivo by using ATAC-seq,[33] a technique sufficiently sensitive to detect these states in the limited number (50 000) of CM nuclei that were isolated from the BZ (Figure 5A). Analysis of the distribution of accessible sites revealed that the majority mapped to intra- and intergenic regions and on average 15 000 to promoters (Figure 5B). In sham-operated mice, promoter accessibility at 3 different time points overlapped for 86% (Figure 5C), indicating that the experiments performed on these tissues were reproducible and peak-calling consistent between samples. Inspection of loci likely to be accessible in CMs confirmed accessible promoters originating from CMs (Figure 5D and 5E).

To determine the correlation between promoter accessibility and gene expression, we integrated the ATAC-seq data with BZ whole tissue RNA-seq data. Because of the observed correlation between accessibility of promoters and expression levels of their respective genes (Figure 5F), we analyzed the dynamic temporal changes in promoter accessibility 4, 7, and 14 dpi. A large number of promoters gained or lost accessibility after injury (Figure 5G), which correlated well with the induction (eg, *Nppa*, *Nppb*) and reduction (eg, *Ryr2*, *Pln*), respectively, of gene expression in the BZ (Figure IX in the online-only Data Supplement). In contrast, promoters of cell cycle genes and of Hippo-, NRG-, BMP-, and Wnt-signaling, implicated in CM renewal and regeneration, did not show consistent changes in accessibility. Cluster analysis of differentially accessible promoters between the BZ and sham CMs indicated at least 5 temporal patterns of changed accessibility (Figure 5H). A large number of promoters of cardiac lineage-specific genes involved in contraction, sarcoplasmic reticulum, ion handling, and calcium signaling became less accessible in the BZ CMs. Promoters of genes involved in angiogenesis and hypoxia response showed an early response but normalized thereafter, whereas other promoters for genes involved in the immune response, wound healing, and extracellular matrix became accessible (Figure 5H).

In addition to promotor accessibility studies, we investigated accessibility patterns of putative regulatory elements (eg, enhancers). Although the majority of signals remained stable between sham and BZ CMs, we identified thousands of sites that either gain or lose accessibility, indicative of profound changes in gene regulation (Figure 6B). Unchanging accessible sites were enriched for CM-specific H3K27ac signatures, indicating that these represent regulatory elements active in both sham and BZ CMs (Figure 6C). Sites displaying decreasing accessibility were enriched for H3K27ac marks, suggesting that regulatory elements active under homeostatic conditions lose activity after injury. In contrast, emerging sites and sites with increasing accessibility were much less frequently marked by H3K27ac, suggesting that these regulatory elements are not typically active in CMs during normal homeostasis (Figure 6C).

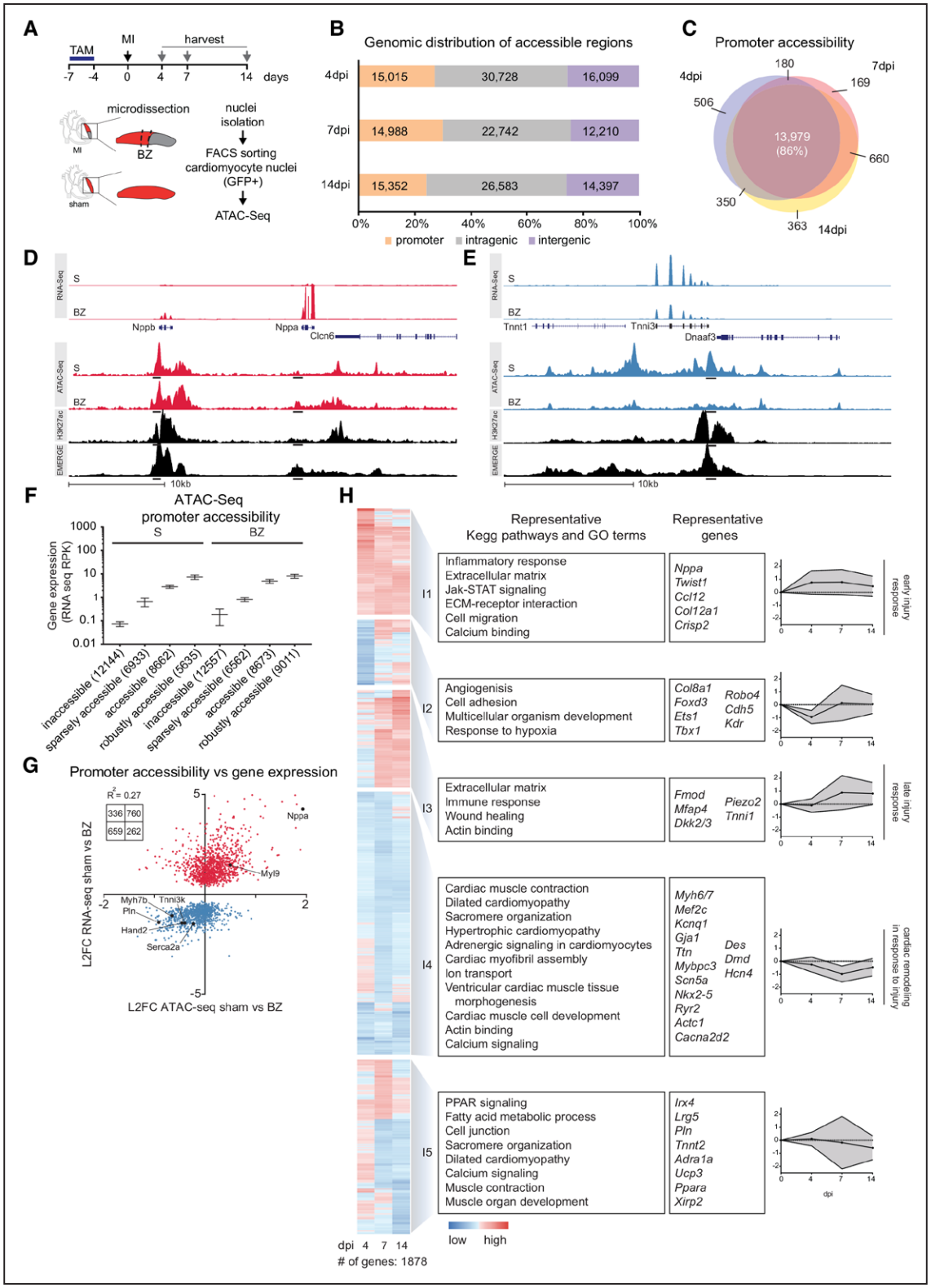

Figure 5. Epigenetic profiling of BZ cardiomyocyte response to injury.
A, Schematic of GFP+ nuclei sorting for ATAC-seq. **B**, Analysis of the distribution of accessible sites, intra- and intergenic regions and promoters, at different time points. **C**, Overlapping promoter accessibility at 3 time points in sham-operated mice (86%) indicated that performed experiments were reproducible. **D** and **E**, Representative loci containing accessible promoters originating from cardiomyocytes. **F**, Dotplot plotting average gene expression levels (RNA-seq RPK) as a function of promoter accessibility (as determined by ATAC-seq). **G**, Scatterplot showing the relation between BZ differential expression (RNA-seq) and BZ differential accessibility of promoters (ATAC-seq). All significantly DE genes (*P* value adjusted for multiple testing: false discovery rate<0.05) between sham and BZ at 7 dpi (RNA-seq) were included. Correlation coefficient and number of genes per quadrant are given. **H**, Functional annotation heatmap showing dynamics of chromatin accessibility of promoters between sham and BZ (n=3 per tissue per time point). ATAC-seq indicates assay for transposase-accessible chromatin using sequencing; BZ, border zone; DE, differential expression; dpi, days postinfarction; GFP, green fluorescent protein; MI, myocardial infarction; RNA-seq, RNA sequencing; RPK, read per kilobase; and TAM, Tamoxifen.

To determine which TFs may interact with the accessibility-enriched or -depleted sites at the 3 time points after MI, we used HOMER to identify enriched sequence motifs potentially recognized by specific transcriptional regulators (Figure 6D and 6E). Both disappearing sites and sites with decreasing accessibility were highly enriched for motifs recognized by members of the Mef2 TF family and, to a lesser extent, by members of the T-box, Meis, and Smad (transforming growth factor β/bone morphogenic protein signaling) TF families. Members of each of these families are involved in cardiogenesis and CM lineage-specific gene regulation.[34] In contrast, both sites with increasing and emerging accessibility were strikingly enriched for motifs recognized by Jun and Fos family members (Figure 6D and 6E).[25] In addition, Runx, Erg, Smad, E-box (MyoD), and TEAD recognition sites were enriched.

To gain insight into the temporal pattern of accessibility, we identified 933 chromatin sites differentially accessible at at least one time point (Figure 6F and Figure X in the online-only Data Supplement). We observed that depleted sites, enriched in recognition sites for Mef2 family members, are less accessible during the onset of pathology, whereas, at a later stage (14 dpi), partially restored their accessibility. In contrast, sites in clusters 5 and 6, highly enriched in AP-1 recognition sites (Jun/Fos), became more accessible after MI and sustained accessibility until at least 14 dpi.

To test whether the motif enrichment results correspond to increased binding, we cross-referenced our different ATAC-seq signal classes (increased, maintained, decreased) with available adult cardiac MEF2[35] and myoblast c-Jun[36] ChIP-seq data. We plotted heart MEF2 ChIP-seq tag abundance per ATAC-seq peak group (Figure 7A and 7B), which shows that regions that become accessible in the BZ have markedly less MEF2 binding. Reduced MEF2 binding could not be attributed to lower expression of *Mef2a*, the main postnatal cardiac isoform,[37] *Mef2c* or *Mef2d,* because BZ CMs readily expressed these genes (Figure 7E and Figure XIE in the online-only Data Supplement and Table III in the online-only Data Supplement). Likewise, we plotted c-Jun (AP-1 component) ChIP-seq tag abundance (Figure 7C), and found that the BZ-enriched peaks show stronger c-Jun binding activity at all measured time points (Figure 7C and 7D). The expression of AP-1 component genes *Jun*, *Junb*, *Jund*, *Fosl1*, and *Fosl2* was increased in BZ CM nuclei in comparison to RM nuclei (Figure 7E and Figure XIE in the online-only Data Supplement and Tables III and IV in the online-only Data Supplement). Furthermore, we detected c-Jun in BZ CM nuclei at 7 and 14 dpi, but not in CM of RM or of sham- operated mice (Figure 7G and Figure XII in the online-only Data Supplement), and we validated the dependency of several of the stress-response enhancer fragments to c-Jun (Figure XIB through XID in the online-only Data Supplement). These data corroborate the motif enrichment findings, and indicate that the CM-specific BZ response is, in part, driven by activated c-Jun.

Taken together, these data suggest that the CM lineage-specific program is downregulated after injury in BZ CMs, involving reduced MEF2 interaction with target regulatory sequences, whereas a stress program is induced by, among others, induced c-Jun (AP-1) activity in the BZ CM nuclei (Figure 7F).

DISCUSSION

In this study, we identified the BZ of the ischemically injured ventricular wall as a transcriptionally discrete compartment distinct from the RM. The observed expression patterns of many novel BZ markers including *Gpx3*, *Clu*, and *Ankrd1* closely matched those of *Nppa*, indicating that a generalized transcriptional BZ compartment forms around the infarct in the mouse heart. In the BZ and, to a much lesser extent, in the RM, we observed a striking and immediate downregulation of genes implicated in cardiac muscle contraction, oxidative phosphorylation, mitochondrial activity, and fatty acid β-oxidation, all of which are specifically highly active in the mature CM lineage. This genome-wide assessment is in agreement with previous studies in which CMs close to the infarct were found to activate *Nppa* (ANF), *Acta2* (aSMA), and *Runx1*, among others, and to show accumulation of lipid droplets, perinuclear sarcomere depletion, and glycogen accumulation.[4,5,13] These changes, however, may also result from stress mechanisms instead of dedifferentiation in the strict developmental sense. For example, the induction of *Nppa, Nppb*, and presumably other genes in adult cardiac stress, often referred to as the activation of the fetal gene program, is achieved through adult stress regulatory DNA sequences that are different from those that activate *Nppa* and *Nppb* during development.[38]

Adult post-MI CMs were reported to not revert back to the neonatal stage.[30] We note, however, that, in these studies, CMs were isolated from whole heart, which mainly comprises RM CMs, because the BZ is but a small fraction of the total cell population. Both our ATAC-seq data and the PCM-1+ CM nuclear expression profiling data revealed a striking absence of induction of cell cycle and glycolysis genes (Figure 5 and Figure IX in the online-only Data Supplement), which were expected to be induced if BZ CMs would revert to the neonatal stage. Indeed, CM cell cycle activity in the BZ after MI is negligible.[15] Furthermore, promoters of genes for signaling pathway components associated with CM proliferation and cardiac regeneration[14–18] were not induced in BZ CMs. Thus, the BZ CMs downregulate mature CM lineage-specific genes but fail to induce neonatal programs for proliferation and metabolic

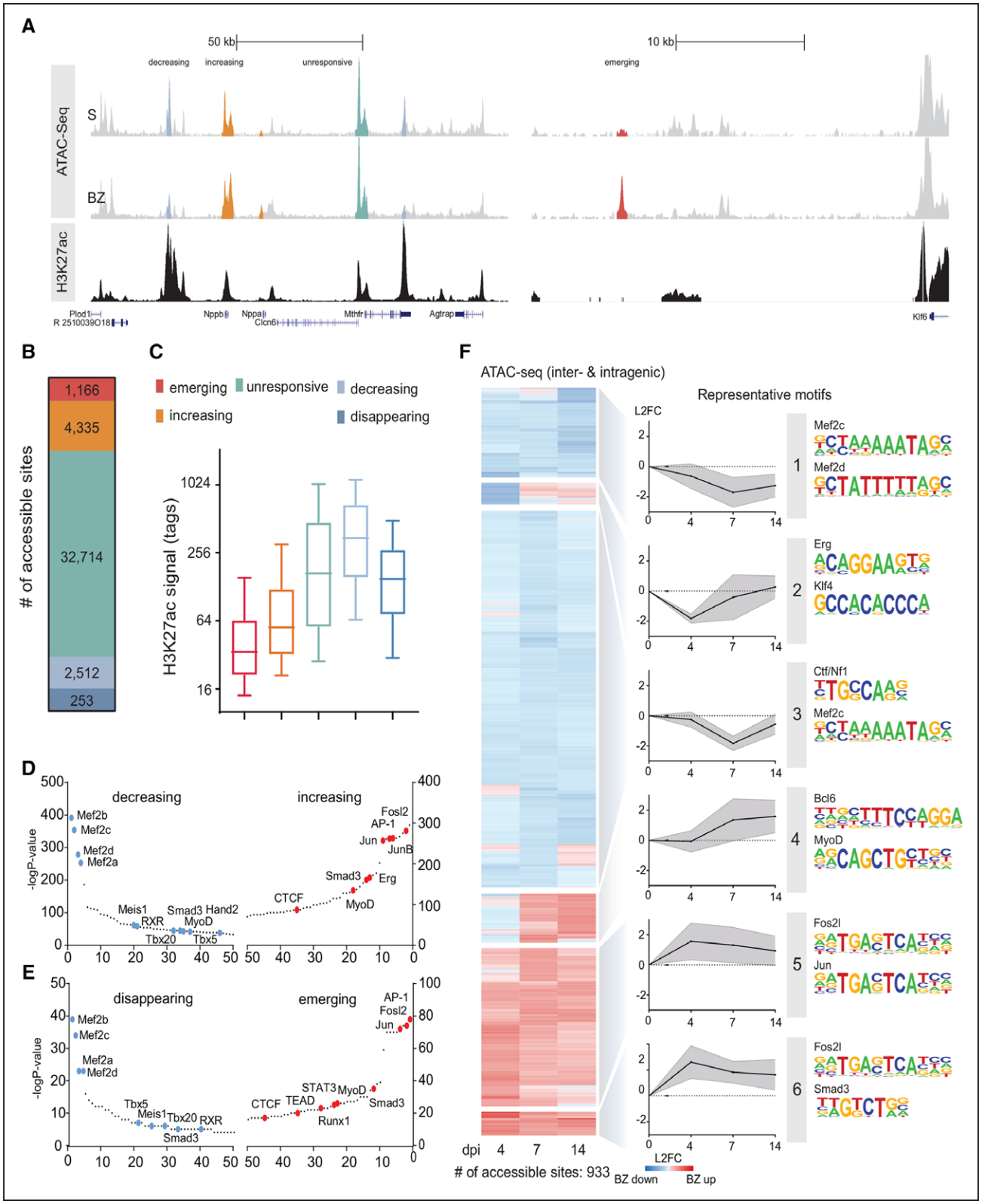

Figure 6. Identification of enriched motifs in BZ cardiomyocytes.
A, Representative inter- and intragenic accessibility patterns, reflecting changes in activity of enhancers and other types of regulatory elements in the BZ. **B**, Distribution of distal accessibility regions across the 5 classes of dynamic peaks. **C**, Box plots showing the intensity of ACM H3K27ac signal (total tags) per dynamic peak class. Enriched transcription factor binding motifs in decreasing and increasing (**D**) and disappearing and emerging (**E**) ATAC-seq peaks, as determined by HOMER, were ranked based on their *P* value. Motifs involved in maintaining the cardiomyocyte lineage homeostasis such as Mef2c, were no longer accessible, whereas AP-1 binding sites gained accessibility. **F**, Hierarchical clustering heatmap of distal accessible regions detectable at all time points (n=3 per tissue per time point) and differentially affected at at least 1 time point. The highest enriched motifs per cluster (as calculated by HOMER) are given. AP-1 indicates activator protein 1; ATAC-seq, assay for transposase-accessible chromatin using sequencing; BZ, border zone; CTCF, CCCTC-binding factor; and dpi, days postinfarction.

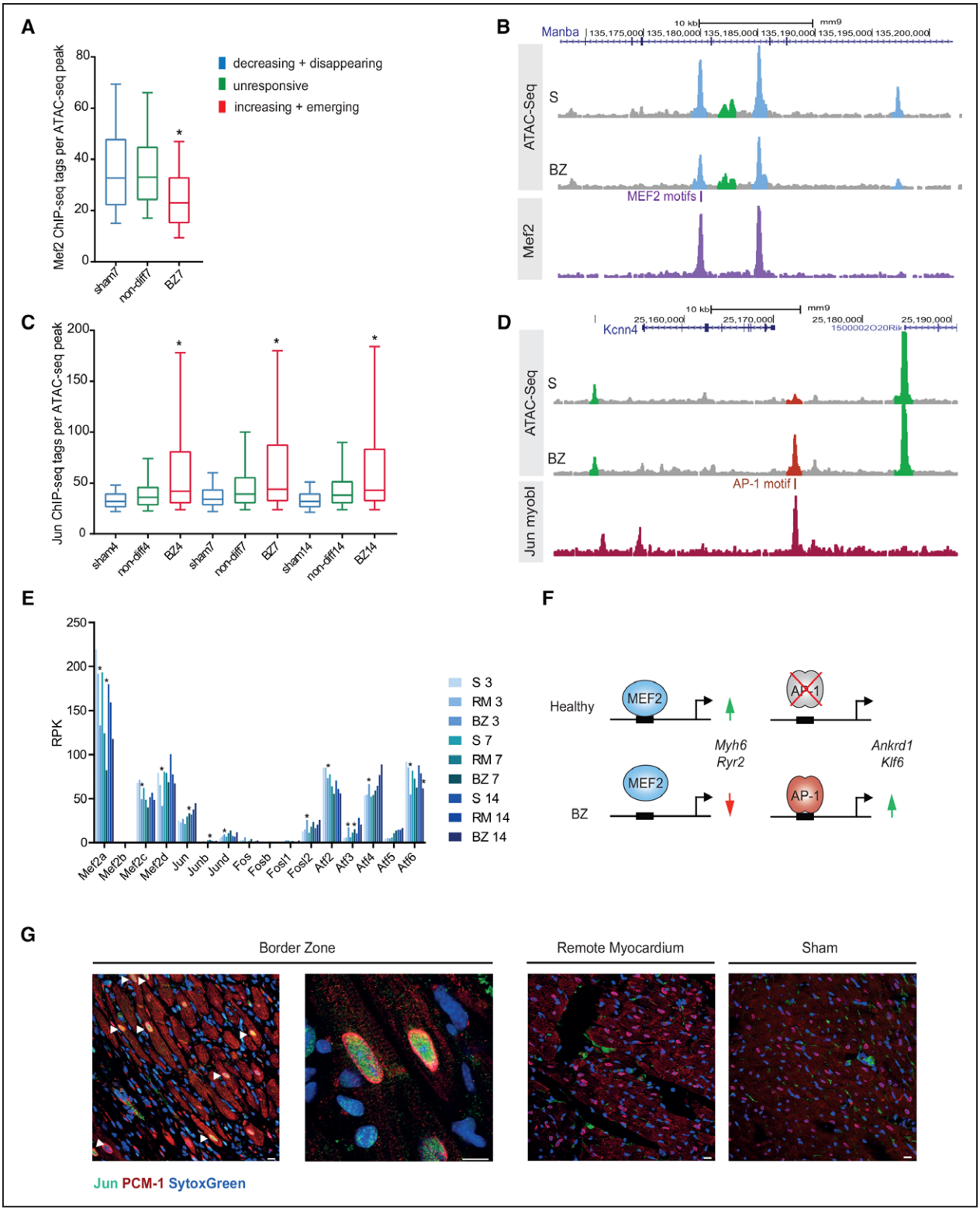

Figure 7. BZ cardiomyocytes are enriched for AP-1 binding motifs.

A, Box plots showing the intensity of MEF2 ChIP-seq signal (total tags) per dynamic peak class at 7 dpi. **B**, Example UCSC Genome Browser view of BZ decreasing accessibility regions that overlap with MEF2 ChIP-seq peaks. A MEF2 consensus motif was found and noted for one of the peaks. **C**, Box plots showing the intensity of Jun ChIP-seq signal (total tags) per dynamic peak class across all measured time points. **D**, Example UCSC Genome Browser view of a BZ emerging accessibility region that overlaps with a Jun ChIP-seq peak, containing a consensus AP-1 motif. **E**, Average RPK values obtained from whole tissue RNA-seq (n=3 per tissue per time point) for the members of the AP-1 family of transcription factors and the Mef2 family of transcription factors. **F**, Cardiac lineage-specific transcription binding sites, such as Mef2, whereas accessibility of non-CM lineage typical promoters/genes and enhancers with binding motifs for AP-1 and other stress responsive transcription factors increases. **G**, Immunohistochemical staining of pericentriolar material 1 (PCM-1), c-Jun, and Sytox Green of BZ, RM, and sham at 7 dpi. Arrowheads indicate c-Jun–positive cardiomyocyte nuclei. Scale bar, 10 μm. *P<0.05 in a 1-way ANOVA. AP-1 indicates activator protein 1; ATAC-seq, assay for transposase-accessible chromatin using sequencing; BZ, border zone; ChIP-seq, chromatin immunoprecipitation sequencing; dpi, days postinfarction; RM, remote myocardium; RPK, read per kilobase; and S, sham.

switching to glycolysis. It is interesting that transgenic mice in which the CM cell cycle is stimulated show CM proliferation after MI preferentially in the BZ,[15–18] suggesting that the dedifferentiated (or stressed) state the BZ CMs acquire after MI is involved but not sufficient for CM renewal after injury.

B-type natriuretic peptide, encoded by *NPPB*, is a widely used biomarker for diagnosis and prognosis in patients with acute or chronic heart failure.[39] Although *Nppb*$^{-/-}$ mice do not show elevated blood pressure or hypertrophy, they were reported to develop cardiac fibrosis from 15 weeks of age onward, which was exaggerated in response to pressure overload.[32,40] Infusion of B-type natriuretic peptide in mice led to arrhythmia and calcium handling alterations in the heart.[41] In contrast, local B-type natriuretic peptide treatment by viral delivery to the heart restored calcium homeostasis in CMs and restored contractility.[42] However, in our mutants, we did not observe changed expression of any of the genes implicated in these processes both before and after MI, indicating they are not predisposed to develop heart failure or fibrosis in response to MI. Further analysis will be required to gain insight into the underlying mechanism and possibly secondary effects such as pulmonary vascular remodeling.[43] The acute development of heart failure and death of *Nppb*$^{-/-}$ mice after MI illustrates the importance of a proper injury response by the BZ after MI. We expect many other vital processes to occur in this region, and the RNA-seq and ATAC-seq data presented here might form the starting point for their discovery. Furthermore, it may be interesting to assess the relation between B-type natriuretic peptide levels and vulnerability to develop complications after MI.

ATAC-seq analysis of CM nuclei revealed that sites losing accessibility after MI were marked by CM-specific acetylated H3K27, a marker for active transcription regulatory sequences (ie, enhancers), and were enriched in motifs for binding of MEF2, although, to a lesser extent, TBX and MEIS families of TFs. The Mef2 family of TFs plays an important role during cardiac development and cardiac hypertrophy.[44,45] *Mef2a* maintains CM differentiation and mitochondrial activity.[37] The reduced accessibility of MEF2-enriched elements in BZ CMs indicates that the Mef2-driven program is downregulated, which is in line with the observed reduction of the mature state and mitochondrial activity of the BZ CMs. In heart failure–induced enhancers (H3K27ac signals), the MEF2 motif is enriched,[46] compatible with the activation of Mef2 function in hypertrophy.[44,45] This suggests that BZ CMs respond oppositely to stress in heart failure and after MI, and indicate that CM lineage-specific enhancers are being inactivated after MI.

Sites that gained accessibility, in contrast, were much less frequently marked by CM-specific H3K27ac, suggesting they were activated de novo in response to MI. These sites were highly enriched in motifs for members of the Jun and Fos families of TFs.[25] *Jun* and *Fosl2* were found to be required for heart development.[26,27] A recent study found that, in skin wound repair, cells lose homeostatic lineage-specific properties when injury-induced stress-responsive enhancers are activated by factors such as AP-1 that override homeostatic regulatory elements governing lineage specificity.[47] Our data indicate that such a mechanism occurs in BZ CMs as well. We observe a massive reduction of accessibility of CM lineage-specific promoters/genes and enhancers with CM lineage-specific TF binding motifs, whereas accessibility of non-CM lineage typical promoters/genes and enhancers with binding motifs for AP-1, TEAD, and other stress-responsive TFs increased (Figure 6D and 6F). The MEF2 and AP-1 motif enrichment results were supported by overlap analysis with available ChIP-seq data and the selective BZ CM nuclear localization of c-Jun (Figure 7).

When the cell cycle is stimulated through cardiac overexpression of, for example cyclin D2, Tbx20, or YAP, CM cycling is observed predominantly in the BZ, suggesting that the phenotype of the BZ CMs is favorable for the stimulation of proliferation.[15,17,18] In mice, direct or indirect activation of nuclear YAP leads to proliferation of both healthy and postinjury CMs.[16,46] YAP interacts with TEAD, a DNA-binding TF, to regulate downstream gene expression.[48] ChIP-seq and ATAC-seq data revealed that YAP-TEAD binding sites are enriched for AP-1 binding sites.[46,49,50] In breast cancer cells, YAP-TEAD was found to associate with AP-1/JUN/FOS at enhancers controlling proliferation.[50] We speculate that the emergence of AP-1 motif enhancers in BZ CMs associated with activation of a stress-responsive gene program creates a favorable state poised for proliferation to occur when YAP-TEAD signaling is activated experimentally in postinjury CMs (Figure XIII in the online-only Data Supplement).

For future targeted therapy, it is relevant to identify and characterize the BZ CMs in the ischemic human heart. In this study, we show that the BZ is transcriptionally conserved between mouse and human and identified novel BZ marker genes. CMs adjacent to both the IZ and endocardium showed strongest expression of these BZ markers. Likely, these cells survive the MI by oxygen and nutrients supplied directly from the ventricular lumen. This region of activated myocardium is important because the CMs in this rim might be most responsive to proliferative stimuli like YAP-TEAD. Furthermore, our data suggest that this responsiveness might be restricted to a temporal window, because the expression of marker genes subsides with the maturation of the scar. For therapeutic purposes, techniques could be developed to target this subendocardial rim of surviving and activated CMs with stimuli to promote regeneration of the human heart.

ARTICLE INFORMATION

Received November 19, 2018; accepted June 20, 2019.

The online-only Data Supplement is available with this article at https://www.ahajournals.org/doi/suppl/10.1161/circulationaha.118.038944.

Correspondence

Vincent M. Christoffels, PhD, Department of Medical Biology, Amsterdam Cardiovascular Sciences, Academic Medical Center, Meibergdreef 15, 1105AZ Amsterdam, The Netherlands; or Jeroen Bakkers, PhD, Hubrecht Institute, University Medical Centre Utrecht, Uppsalalaan 8, 3584CT Utrecht, The Netherlands. Email v.m.christoffels@amc.uva.nl or j.bakkers@hubrecht.eu

Affiliations

Departments of Medical Biology, Amsterdam Cardiovascular Sciences (K.v.D., J.C.K.M., R.J., M.G., I.B.H., P.B., V.M.C.) and Experimental Cardiology (I.v.d.M., E.E.C.), Academic Medical Center, Amsterdam, The Netherlands. Hubrecht Institute (D.E.M.d.B., J.B.), Department of Pathology (P.H.v.d.K., A.V.), University Medical Centre Utrecht, The Netherlands. Program in Developmental Biology (M.C.H., J.F.M.) and Department of Molecular Physiology and Biophysics (J.F.M.), Baylor College of Medicine, Houston, TX.

Acknowledgments

We thank C. de Gier-de Vries for help with the in situ hybridizations.

Sources of Funding

This study was supported by Netherlands Heart Foundation COBRA3 and Cardiovasculair Onderzoek Nederland HUSTCARE to Drs Christoffels and Bakkers, a European Research Area Network-Cardiovascular Diseases CARDIOPRO grant to Dr Bakkers, and a Leducq Foundation grant (14CVD01) to Dr Christoffels.

Disclosures

None.

REFERENCES

1. Bergmann O, Zdunek S, Felker A, Salehpour M, Alkass K, Bernard S, Sjostrom SL, Szewczykowska M, Jackowska T, Dos Remedios C, et al. Dynamics of cell generation and turnover in the human heart. *Cell.* 2015;161:1566–1575. doi: 10.1016/j.cell.2015.05.026
2. Factor SM, Sonnenblick EH, Kirk ES. The histologic border zone of acute myocardial infarction–islands or peninsulas? *Am J Pathol.* 1978;92:111–124.
3. Driesen RB, Verheyen FK, Dijkstra P, Thoné F, Cleutjens JP, Lenders MH, Ramaekers FC, Borgers M. Structural remodelling of cardiomyocytes in the border zone of infarcted rabbit heart. *Mol Cell Biochem.* 2007;302:225–232. doi: 10.1007/s11010-007-9445-2
4. Sharov VG, Sabbah HN, Ali AS, Shimoyama H, Lesch M, Goldstein S. Abnormalities of cardiocytes in regions bordering fibrous scars of dogs with heart failure. *Int J Cardiol.* 1997;60:273–279.
5. Dispersyn GD, Mesotten L, Meuris B, Maes A, Mortelmans L, Flameng W, Ramaekers F, Borgers M. Dissociation of cardiomyocyte apoptosis and dedifferentiation in infarct border zones. *Eur Heart J.* 2002;23:849–857. doi: 10.1053/euhj.2001.2963
6. Ounzain S, Micheletti R, Beckmann T, Schroen B, Alexanian M, Pezzuto I, Crippa S, Nemir M, Sarre A, Johnson R, et al. Genome-wide profiling of the cardiac transcriptome after myocardial infarction identifies novel heart-specific long non-coding RNAs. *Eur Heart J.* 2015;36:353–68a. doi: 10.1093/eurheartj/ehu180
7. Kaikkonen MU, Halonen P, Liu OH, Turunen TA, Pajula J, Moreau P, Selvarajan I, Tuomainen T, Aavik E, Tavi P, et al. Genome-wide dynamics of nascent noncoding RNA transcription in porcine heart after myocardial infarction. *Circ Cardiovasc Genet.* 2017;10:1–11.
8. Lacraz GPA, Junker JP, Gladka MM, Molenaar B, Scholman KT, Vigil-Garcia M, Versteeg D, de Ruiter H, Vermunt MW, Creyghton MP, et al. Tomo-Seq identifies SOX9 as a key regulator of cardiac fibrosis during ischemic injury. *Circulation.* 2017;136:1396–1409. doi: 10.1161/CIRCULATIONAHA.117.027832
9. Gladka MM, Molenaar B, de Ruiter H, van der Elst S, Tsui H, Versteeg D, Lacraz GPA, Huibers MMH, van Oudenaarden A, van Rooij E. Single-cell sequencing of the healthy and diseased heart reveals cytoskeleton-associated protein 4 as a new modulator of fibroblasts activation. *Circulation.* 2018;138:166–180. doi: 10.1161/CIRCULATIONAHA.117.030742
10. Jackson BM, Gorman JH, Moainie SL, Guy TS, Narula N, Narula J, John-Sutton MG, Edmunds LH Jr, Gorman RC. Extension of border-zone myocardium in postinfarction dilated cardiomyopathy. *J Am Coll Cardiol.* 2002;40:1160–1167; discussion 1168. doi: 10.1016/s0735-1097(02)02121-6
11. de Bakker JM, van Capelle FJ, Janse MJ, Wilde AA, Coronel R, Becker AE, Dingemans KP, van Hemel NM, Hauer RN. Reentry as a cause of ventricular tachycardia in patients with chronic ischemic heart disease: electrophysiologic and anatomic correlation. *Circulation.* 1988;77:589–606. doi: 10.1161/01.cir.77.3.589
12. Francis Stuart SD, De Jesus NM, Lindsey ML, Ripplinger CM. The crossroads of inflammation, fibrosis, and arrhythmia following myocardial infarction. *J Mol Cell Cardiol.* 2016;91:114–122. doi: 10.1016/j.yjmcc.2015.12.024
13. Ursell PC, Gardner PI, Albala A, Fenoglio JJ Jr, Wit AL. Structural and electrophysiological changes in the epicardial border zone of canine myocardial infarcts during infarct healing. *Circ Res.* 1985;56:436–451. doi: 10.1161/01.res.56.3.436
14. Wu CC, Kruse F, Vasudevarao MD, Junker JP, Zebrowski DC, Fischer K, Noël ES, Grün D, Berezikov E, Engel FB, et al. Spatially resolved genome-wide transcriptional profiling identifies BMP signaling as essential regulator of zebrafish cardiomyocyte regeneration. *Dev Cell.* 2016;36:36–49. doi: 10.1016/j.devcel.2015.12.010
15. Pasumarthi KB, Nakajima H, Nakajima HO, Soonpaa MH, Field LJ. Targeted expression of cyclin D2 results in cardiomyocyte DNA synthesis and infarct regression in transgenic mice. *Circ Res.* 2005;96:110–118. doi: 10.1161/01.RES.0000152326.91223.4F
16. Leach JP, Heallen T, Zhang M, Rahmani M, Morikawa Y, Hill MC, Segura A, Willerson JT, Martin JF. Hippo pathway deficiency reverses systolic heart failure after infarction. *Nature.* 2017;550:260–264. doi: 10.1038/nature24045
17. Xiang FL, Guo M, Yutzey KE. Overexpression of Tbx20 in adult cardiomyocytes promotes proliferation and improves cardiac function after myocardial infarction. *Circulation.* 2016;133:1081–1092. doi: 10.1161/CIRCULATIONAHA.115.019357
18. Lin Z, von Gise A, Zhou P, Gu F, Ma Q, Jiang J, Yau AL, Buck JN, Gouin KA, van Gorp PR, et al. Cardiac-specific YAP activation improves cardiac function and survival in an experimental murine MI model. *Circ Res.* 2014;115:354–363. doi: 10.1161/CIRCRESAHA.115.303632
19. Sergeeva IA, Hooijkaas IB, Van Der Made I, Jong WM, Creemers EE, Christoffels VM. A transgenic mouse model for the simultaneous monitoring of ANF and BNP gene activity during heart development and disease. *Cardiovasc Res.* 2014;101:78–86. doi: 10.1093/cvr/cvt228
20. Sohal DS, Nghiem M, Crackower MA, Witt SA, Kimball TR, Tymitz KM, Penninger JM, Molkentin JD. Temporally regulated and tissue-specific gene manipulations in the adult and embryonic heart using a tamoxifen-inducible Cre protein. *Circ Res.* 2001;89:20–25. doi: 10.1161/hh1301.092687
21. Love MI, Huber W, Anders S. Moderated estimation of fold change and dispersion for RNA-seq data with DESeq2. *Genome Biol.* 2014;15:550. doi: 10.1186/s13059-014-0550-8
22. Heinz S, Benner C, Spann N, Bertolino E, Lin YC, Laslo P, Cheng JX, Murre C, Singh H, Glass CK. Simple combinations of lineage-determining transcription factors prime cis-regulatory elements required for macrophage and B cell identities. *Mol Cell.* 2010;38:576–589. doi: 10.1016/j.molcel.2010.05.004
23. Frangogiannis NG. The inflammatory response in myocardial injury, repair, and remodelling. *Nat Rev Cardiol.* 2014;11:255–265. doi: 10.1038/nrcardio.2014.28
24. Fu X, Khalil H, Kanisicak O, Boyer JG, Vagnozzi RJ, Maliken BD, Sargent MA, Prasad V, Valiente-Alandi I, Blaxall BC, et al. Specialized fibroblast differentiated states underlie scar formation in the infarcted mouse heart. *J Clin Invest.* 2018;128:2127–2143. doi: 10.1172/JCI98215
25. Hess J, Angel P, Schorpp-Kistner M. AP-1 subunits: quarrel and harmony among siblings. *J Cell Sci.* 2004;117(pt 25):5965–5973. doi: 10.1242/jcs.01589
26. Eferl R, Sibilia M, Hilberg F, Fuchsbichler A, Kufferath I, Guertl B, Zenz R, Wagner EF, Zatloukal K. Functions of c-Jun in liver and heart development. *J Cell Biol.* 1999;145:1049–1061. doi: 10.1083/jcb.145.5.1049
27. Jahangiri L, Sharpe M, Novikov N, González-Rosa JM, Borikova A, Nevis K, Paffett-Lugassy N, Zhao L, Adams M, Guner-Ataman B, et al. The AP-1

transcription factor component Fosl2 potentiates the rate of myocardial differentiation from the zebrafish second heart field. *Development*. 2016;143:113–122. doi: 10.1242/dev.126136
28. Pinto AR, Ilinykh A, Ivey MJ, Kuwabara JT, D'Antoni ML, Debuque R, Chandran A, Wang L, Arora K, Rosenthal NA, et al. Revisiting cardiac cellular composition. *Circ Res.* 2016;118:400–409. doi: 10.1161/CIRCRESAHA.115.307778
29. Preissl S, Schwaderer M, Raulf A, Hesse M, Grüning BA, Köbele C, Backofen R, Fleischmann BK, Hein L, Gilsbach R. Deciphering the epigenetic code of cardiac myocyte transcription. *Circ Res.* 2015;117:413–423. doi: 10.1161/CIRCRESAHA.115.306337
30. Quaife-Ryan GA, Sim CB, Ziemann M, Kaspi A, Rafehi H, Ramialison M, El-Osta A, Hudson JE, Porrello ER. Multicellular transcriptional analysis of mammalian heart regeneration. *Circulation.* 2017;136:1123–1139. doi: 10.1161/CIRCULATIONAHA.117.028252
31. Jenkins CP, Cardona DM, Bowers JN, Oliai BR, Allan RW, Normann SJ. The utility of C4d, C9, and troponin T immunohistochemistry in acute myocardial infarction. *Arch Pathol Lab Med.* 2010;134:256–263. doi: 10.1043/1543-2165-134.2.256
32. Tamura N, Ogawa Y, Chusho H, Nakamura K, Nakao K, Suda M, Kasahara M, Hashimoto R, Katsuura G, Mukoyama M, et al. Cardiac fibrosis in mice lacking brain natriuretic peptide. *Proc Natl Acad Sci U S A.* 2000;97:4239–4244. doi: 10.1073/pnas.070371497
33. Buenrostro JD, Giresi PG, Zaba LC, Chang HY, Greenleaf WJ. Transposition of native chromatin for fast and sensitive epigenomic profiling of open chromatin, DNA-binding proteins and nucleosome position. *Nat Methods.* 2013;10:1213–1218. doi: 10.1038/nmeth.2688
34. Liu Q, Jiang C, Xu J, Zhao MT, Van Bortle K, Cheng X, Wang G, Chang HY, Wu JC, Snyder MP. Genome-wide temporal profiling of transcriptome and open chromatin of early cardiomyocyte differentiation derived from hiPSCs and hESCs. *Circ Res.* 2017;121:376–391. doi: 10.1161/CIRCRESAHA.116.310456
35. Guo A, Wang Y, Chen B, Wang Y, Yuan J, Zhang L, Hall D, Wu J, Shi Y, Zhu Q, et al. E-C coupling structural protein junctophilin-2 encodes a stress-adaptive transcription regulator. *Science*. 2018;362:1–9.
36. Umansky KB, Feldmesser E, Groner Y. Genomic-wide transcriptional profiling in primary myoblasts reveals Runx1-regulated genes in muscle regeneration. *Genom Data.* 2015;6:120–122. doi: 10.1016/j.gdata.2015.08.030
37. Naya FJ, Black BL, Wu H, Bassel-Duby R, Richardson JA, Hill JA, Olson EN. Mitochondrial deficiency and cardiac sudden death in mice lacking the MEF2A transcription factor. *Nat Med.* 2002;8:1303–1309. doi: 10.1038/nm789
38. Sergeeva IA, Hooijkaas IB, Ruijter JM, van der Made I, de Groot NE, van de Werken HJ, Creemers EE, Christoffels VM. Identification of a regulatory domain controlling the Nppa-Nppb gene cluster during heart development and stress. *Development.* 2016;143:2135–2146. doi: 10.1242/dev.132019
39. Ponikowski P, Voors AA, Anker SD, Bueno H, Cleland JGF, Coats AJS, Falk V, González-Juanatey JR, Harjola VP, Jankowska EA, et al; ESC Scientific Document Group. 2016 ESC Guidelines for the diagnosis and treatment of acute and chronic heart failure: The Task Force for the diagnosis and treatment of acute and chronic heart failure of the European Society of Cardiology (ESC) developed with the special contribution of the Heart Failure Association (HFA) of the ESC. *Eur Heart J.* 2016;37:2129–2200. doi: 10.1093/eurheartj/ehw128
40. Holditch SJ, Schreiber CA, Nini R, Tonne JM, Peng KW, Geurts A, Jacob HJ, Burnett JC, Cataliotti A, Ikeda Y. B-Type natriuretic peptide deletion leads to progressive hypertension, associated organ damage, and reduced survival: novel model for human hypertension. *Hypertension.* 2015;66:199–210. doi: 10.1161/HYPERTENSIONAHA.115.05610
41. Thireau J, Karam S, Fauconnier J, Roberge S, Cassan C, Cazorla O, Aimond F, Lacampagne A, Babuty D, Richard S. Functional evidence for an active role of B-type natriuretic peptide in cardiac remodelling and pro-arrhythmogenicity. *Cardiovasc Res.* 2012;95:59–68. doi: 10.1093/cvr/cvs167
42. Moilanen AM, Rysä J, Mustonen E, Serpi R, Aro J, Tokola H, Leskinen H, Manninen A, Levijoki J, Vuolteenaho O, et al. Intramyocardial BNP gene delivery improves cardiac function through distinct context-dependent mechanisms. *Circ Heart Fail.* 2011;4:483–495. doi: 10.1161/CIRCHEARTFAILURE.110.958033
43. Casserly B, Klinger JR. Brain natriuretic peptide in pulmonary arterial hypertension: biomarker and potential therapeutic agent. *Drug Des Devel Ther.* 2009;3:269–287.
44. Desjardins CA, Naya FJ. The function of the MEF2 family of transcription factors in cardiac development, cardiogenomics, and direct reprogramming. *J Cardiovasc Dev Dis*. 2016;3:1–19.
45. Wei J, Joshi S, Speransky S, Crowley C, Jayathilaka N, Lei X, Wu Y, Gai D, Jain S, Hoosien M, et al. Reversal of pathological cardiac hypertrophy via the MEF2-coregulator interface. *JCI Insight*. 2017;2:1–16.
46. Monroe TO, Hill MC, Morikawa Y, Leach JP, Heallen T, Cao S, Krijger PHL, de Laat W, Wehrens XHT, Rodney GG, et al. YAP partially reprograms chromatin accessibility to directly induce adult cardiogenesis in vivo. *Dev Cell.* 2019;48:765–779.e7. doi: 10.1016/j.devcel.2019.01.017
47. Ge Y, Gomez NC, Adam RC, Nikolova M, Yang H, Verma A, Lu CP, Polak L, Yuan S, Elemento O, et al. Stem cell lineage infidelity drives wound repair and cancer. *Cell.* 2017;169:636–650.e14. doi: 10.1016/j.cell.2017.03.042
48. Piccolo S, Dupont S, Cordenonsi M. The biology of YAP/TAZ: hippo signaling and beyond. *Physiol Rev.* 2014;94:1287–1312. doi: 10.1152/physrev.00005.2014
49. Stein C, Bardet AF, Roma G, Bergling S, Clay I, Ruchti A, Agarinis C, Schmelzle T, Bouwmeester T, Schübeler D, et al. YAP1 exerts its transcriptional control via TEAD-mediated activation of enhancers. *PLoS Genet.* 2015;11:e1005465. doi: 10.1371/journal.pgen.1005465
50. Zanconato F, Forcato M, Battilana G, Azzolin L, Quaranta E, Bodega B, Rosato A, Bicciato S, Cordenonsi M, Piccolo S. Genome-wide association between YAP/TAZ/TEAD and AP-1 at enhancers drives oncogenic growth. *Nat Cell Biol.* 2015;17:1218–1227. doi: 10.1038/ncb3216